Molecular Microbiology (2014) 93(5), 897–910 ■
doi:10.1111/mmi.12706
First published online 23 July 2014

Cytosolic iron-sulphur protein assembly is functionally conserved and essential in procyclic and bloodstream *Trypanosoma brucei*

Somsuvro Basu,[1,2] Daili J. Netz,[3,4] Alexander C. Haindrich,[2] Nils Herlerth,[3,4] Thibaut J. Lagny,[3] Antonio J. Pierik,[3,5*] Roland Lill[3,4,6**] and Julius Lukeš[1,2*]**

[1]*Biology Centre, Institute of Parasitology, 37005 České Budějovice (Budweis), Czech Republic.*
[2]*Faculty of Sciences, University of South Bohemia, 37005 České Budějovice (Budweis), Czech Republic.*
[3]*Institut für Zytobiologie und Zytopathologie, Philipps-Universität, 35033 Marburg, Germany.*
[4]*Max-Planck-Institut für terrestrische Mikrobiologie, 35043 Marburg, Germany.*
[5]*Faculty of Chemistry – Biochemistry, University of Kaiserslautern, 67663 Kaiserslautern, Germany.*
[6]*LOEWE Zentrum für Synthetische Mikrobiologie SynMikro, 35043 Marburg, Germany.*

Summary

Cytosolic and nuclear iron-sulphur (Fe/S) proteins include essential components involved in protein translation, DNA synthesis and DNA repair. In yeast and human cells, assembly of their Fe/S cofactor is accomplished by the CIA (cytosolic iron-sulphur protein assembly) machinery comprised of some 10 proteins. To investigate the extent of conservation of the CIA pathway, we examined its importance in the early-branching eukaryote *Trypanosoma brucei* that encodes all known CIA factors. Upon RNAi-mediated ablation of individual, early-acting CIA proteins, no major defects were observed in both procyclic and bloodstream stages. In contrast, parallel depletion of two CIA components was lethal, and severely diminished cytosolic aconitase activity lending support for a direct role of the CIA proteins in cytosolic Fe/S protein biogenesis. In support of this conclusion, the *T. brucei* CIA proteins complemented the growth defects of their respective yeast CIA depletion mutants. Finally, the *T. brucei* CIA factor Tah18 was characterized as a flavoprotein, while its binding partner Dre2 functions as a Fe/S protein. Together, our results demonstrate the essential and conserved function of the CIA pathway in cytosolic Fe/S protein assembly in both developmental stages of this representative of supergroup Excavata.

Accepted 2 July, 2014. For correspondence. *E-mail jula@paru.cas.cz; Tel. (+420) 38 7775416; Fax (+420) 38 5310388; **E-mail lill@staff.uni-marburg.de; Tel. (+49) 6421 2866449; Fax (+49) 6421 2866414; ***E-mail pierik@chemie.uni-kl.de; Tel. (+49) 631 205 4953; Fax (+49) 631 205 3419.

© 2014 John Wiley & Sons Ltd

Introduction

Iron-sulphur (Fe/S) clusters are ancient prosthetic groups present in each realm of life, where they participate in myriads of central biological processes. Their chemical and structural flexibility made them distinctive in function, which spans from respiration, amino acid metabolism, DNA replication to DNA repair (Rudolf *et al.*, 2006; Klinge *et al.*, 2007; Yeeles *et al.*, 2009; Netz *et al.*, 2011). Fe/S protein biogenesis is an indispensable process, highly conserved from bacteria to unicellular and multicellular eukaryotes (Lill, 2009; Roche *et al.*, 2013). So far, three systems have been recognized in bacteria, namely the nitrogen fixing (NIF), sulphur mobilization (SUF) and iron-sulphur cluster (ISC) systems. In the course of evolution, the ISC and SUF systems were laterally transferred to eukaryotes, where they are confined to the mitochondria and plastids respectively. While maturation of the cytosolic and nuclear Fe/S proteins depends on the dedicated eukaryote-only cytosolic Fe/S cluster assembly (CIA), it also requires the sustenance of the ISC assembly and the ISC export machinery (for review see Lill, 2009).

The ISC-export machinery, composed of the mitochondrial inner-membrane ABC transporter Atm1 (Kispal *et al.*, 1999), the inter-membrane space sulphydryl oxidase Erv1 (Lange *et al.*, 2001) and glutathione (Sipos *et al.*, 2002), connects ISC and CIA machineries by exporting a glutathione- and sulphur-containing compound utilized downstream in the cytosol (Srinivasan *et al.*, 2014) (Fig. 1A). The CIA system has been extensively studied in *Saccharomyces cerevisiae*, *Arabidopsis thaliana*, and humans, unveiling the involvement of at least nine proteins (Netz *et al.*, 2014). Initially, Fe/S clusters are assembled on the scaffold complex formed by Cfd1 and Nbp35 (Roy

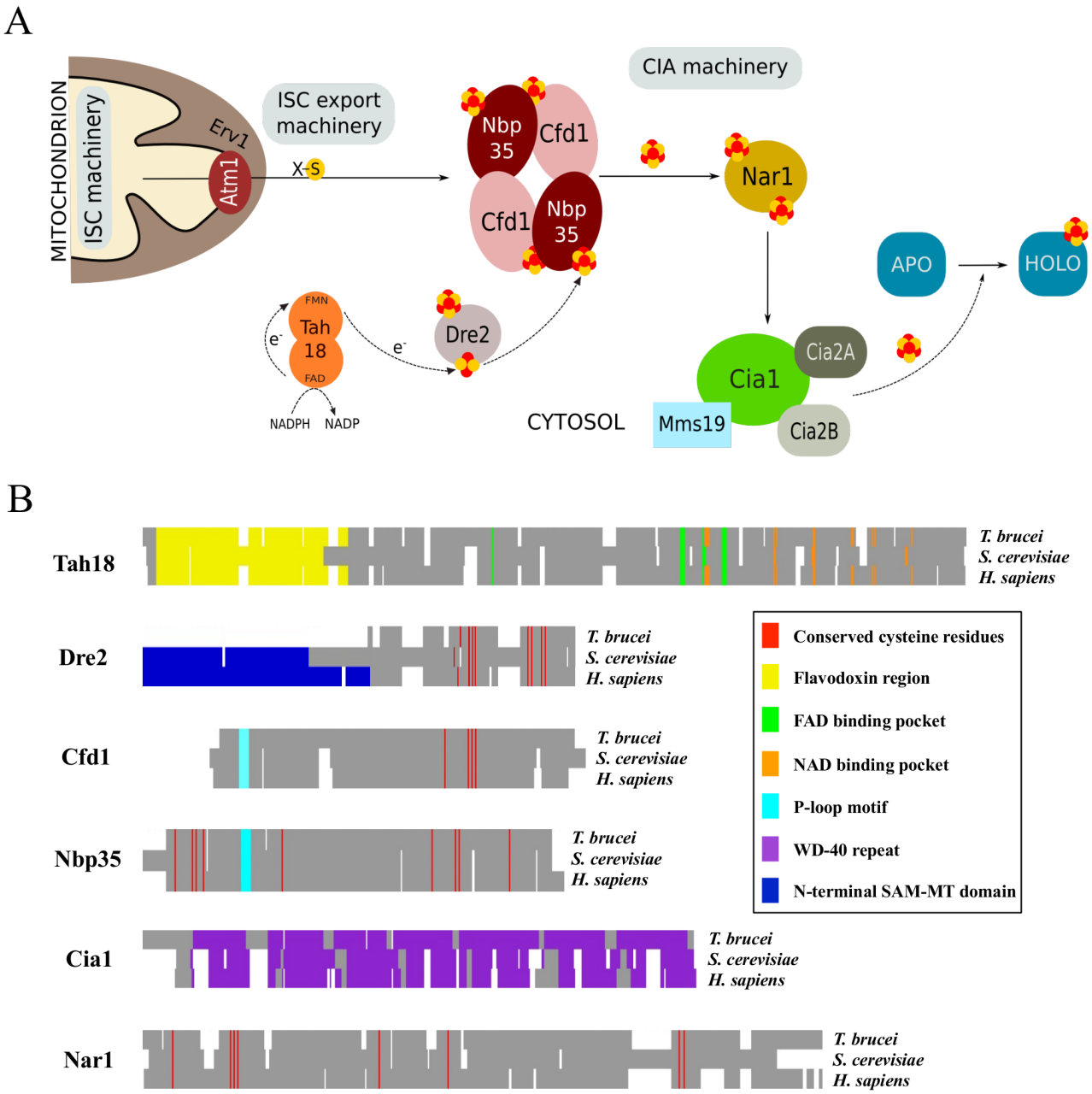

Fig. 1. Current model of the CIA pathway and domain architecture of CIA proteins.
A. The overall organization of the CIA pathway as derived from studies in yeast and human cells is depicted: Fe-S clusters are assembled on the Cfd1/Nbp35 scaffold protein complex with the help of the electron transport chain Tah18/Dre2. Clusters are transferred to the apoproteins via Nar1 and the targeting complex formed by Cia1, Cia2A, Cia2B and Mms19. X-S is the unknown glutathione- and sulphur-containing substrate exported by mitochondrial Atm1.
B. The conserved domain architectures of the CIA candidates involved in the early and intermediate part of the pathway in *T. brucei, S. cerevisiae* and humans are shown in cartoons. The conserved motifs are specified in the accompanying box.

et al., 2003; Netz *et al.*, 2007) from which they are transferred to the apo-proteins via Nar1, itself an Fe/S cluster-containing protein (Balk *et al.*, 2004), and Cia1, a WD40 repeat domain protein, which assists as a platform for interactions with other CIA proteins (Balk *et al.*, 2005) (Fig. 1A). Additionally, Tah18, a diflavin reductase, along with another Fe/S cluster-containing protein Dre2, constitute an electron transfer chain conveying electrons from NADPH through Tah18 to the Dre2-bound Fe/S cluster. This process is required for Nbp35 function and, consequently, downstream Fe/S protein assembly (Netz *et al.*, 2010). The recently observed 'CIA-targeting complex', in

human cells formed by CIA1, MMS19, and CIA2B (Fam96B), transfers the Fe/S clusters to various apoproteins in a target-specific fashion (Balk *et al*., 2005; Netz *et al*., 2010; Gari *et al*., 2012; Stehling *et al*., 2012). Moreover, CIA2A (Fam96A), which is related to CIA2B, is dedicated to maturation of iron regulatory protein 1 (IRP1) thus impacting on cellular iron homeostasis (Stehling *et al*., 2013).

In this study, we scrutinized the CIA pathway in the protist *Trypanosoma brucei*, the causative agent of the devastating human African sleeping sickness and numerous other diseases of mammals. Throughout its life cycle, the parasite switches between two morphologically similar but biochemically distinct stages, the insect-dwelling procyclic stage (PS) and the mammalian bloodstream stage (BS) (Lukeš *et al*., 2005). Due to the functionality of most reverse and forward genetics tools, *T. brucei* became a model organism, representing the eukaryotic superdomain Excavata (Montagnes *et al*., 2012).

In terms of composition and function, the ISC assembly and export machineries are conserved in *T. brucei*, which lacks the SUF and NIF systems (Smíd *et al*., 2006; Paris *et al*., 2010; Long *et al*., 2011; Basu *et al*., 2013). In the PS of *T. brucei*, the ISC system initiates with cysteine desulphurase Nfs1 and the scaffold protein Isu1, both being essential for Fe/S cluster biosynthesis (Smíd *et al*., 2006). Another conserved component, Isd11, was shown to be a binding partner of Nfs1 and, apart from its role in Fe/S cluster assembly, its ablation disrupted both mitochondrial and cytosolic tRNA thiolation (Paris *et al*., 2010). Due to an exceptionally low demand for mitochondrial Fe/S cluster-containing proteins in the BS that does not require the respiratory complexes, both *T. brucei* Isa homologues are dispensable in this stage, but not in the PS flagellates, which carry a respiratory-active organelle (Long *et al*., 2011). Trypanosomes also possess two homologues of ferredoxin, with ferredoxin A being an essential component of the Fe/S cluster biogenesis in both life cycle stages, while the function of ferredoxin B remains unknown (Changmai *et al*., 2013).

Virtually no information is available on the *T. brucei* CIA machinery, although it has been shown recently that its genome encodes homologues of Cfd1 and Nbp35 (Bruske *et al*., 2009; Basu *et al*., 2013), as well as Nar1, Dre2, Tah18 and Mms19 (Ali and Nozaki, 2013; Basu *et al*., 2013) (Fig. 1A).

In this work we focused on functional analysis of the early and middle part of the CIA machinery, which includes TbNbp35, TbCfd1, TbTah18, TbDre2, TbNar1 and TbCia1. We have generated RNAi single knock-down cells for each of these CIA pathway components that unexpectedly did not show detectable growth phenotypes, whereas ablation of two components in parallel was invariably detrimental. Complementation of several yeast CIA mutants with *T. brucei* orthologues indicated high functional conservation of the pathway across eukaryotic supergroups.

Results

Identification of T. brucei *CIA components*

The *S. cerevisiae* and human CIA protein sequences have been used as query for a search of the *T. brucei* genome. We identified all known CIA components, which have been summarized in Table S1. Their conservation with respect to their selected unikont orthologues is shown in detail in Fig. S1. Based on the conservation, a cartoon designating the conserved domain architecture of the CIA components of *T. brucei, S. cerevisiae* and *Homo sapiens* is shown in Fig. 1B.

Most CIA components appear dispensable for cell growth upon RNAi single knock-down

In order to functionally analyse the CIA candidates, we performed individual RNAi-mediated depletions of TbCfd1, TbNbp35, TbTah18, TbDre2, TbNar1 and TbCia1. Fragments of TbCfd1 and TbNbp35 were cloned in the pLew-100-based vector (Bruske *et al*., 2009). Fragments of the other genes (535 bp of TbTah18, 312 bp of TbDre2, 464 bp of TbNar1 and 324 bp of TbCia1) were cloned into the p2T7-177 vector with opposing Tet-regulatable T7 promoters. Upon verification by sequencing, the constructs were separately electroporated into the parental *T. brucei* 29-13 PF and 427 BF cells, and subsequently clonal cell lines were chosen for further analysis under phleomycin selection.

Apart from TbCfd1 and TbNbp35, on which transient Fe/S clusters are thought to be primarily assembled, protein depletion of the other tested CIA components did not interfere with cellular growth rate. The cumulative cell density was equally unaffected, although efficient protein depletion was achieved by RNAi (Fig. 2). Intriguingly, RNAi-mediated ablation of TbCfd1 massively impaired growth in the PS, but only marginally affected the BS cells growth. TbTah18, TbDre2, TbNar1 and TbCia1 RNAi-induced cells showed no significant growth phenotype when compared to their non-induced counterparts in both cell cycle stages (Fig. 2).

Decreased cytosolic but not mitochondrial aconitase activity

The majority of the aconitase activity (70%) is found in the cytosol of *T. brucei*, with the remainder in the single mitochondrion (Saas *et al*., 2000). After efficient subcellular fractionation, the respective activities of aconitase (encoded by a single gene) can be utilized for the measurements of Fe/S cluster assembly in both compartments

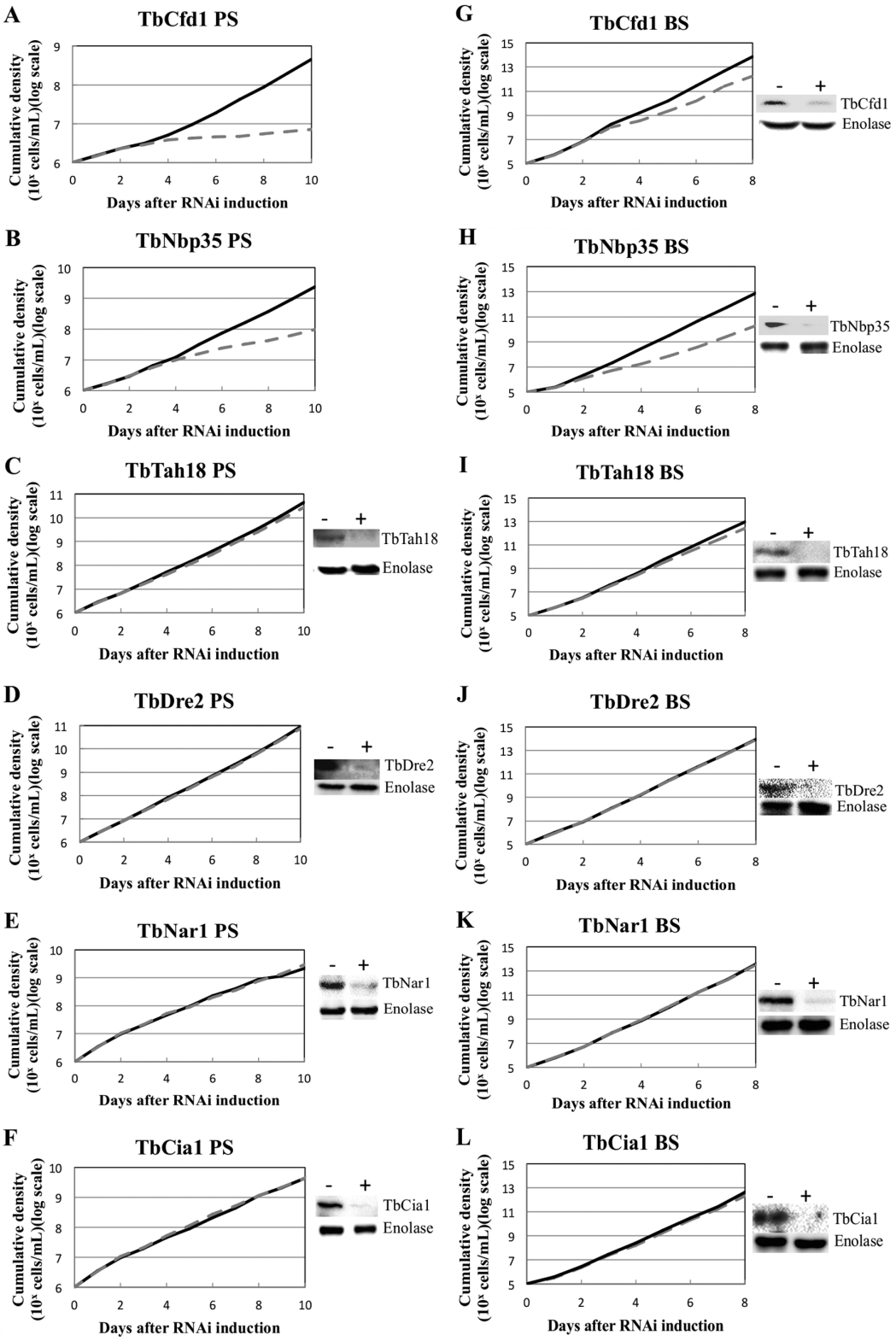

Fig. 2. Depletion of *T. brucei* CIA components and resulting growth behaviour. Growth of procyclic (PS; A–F) and bloodstream (BS) *T. brucei* RNAi cell lines (G–L); the curves of the non-induced (solid lines) and RNAi-induced cells (broken lines) are accompanied by respective Western blots showing the depletion of the targeted proteins upon RNAi induction. The Western blots were performed on the sixth and third day after RNAi induction for the PS (C–F) and BS (G–L) respectively. RNAi validation for PS TbCfd1 (A) and TbNbp35 (B) has been shown in Bruske *et al.* (2009).

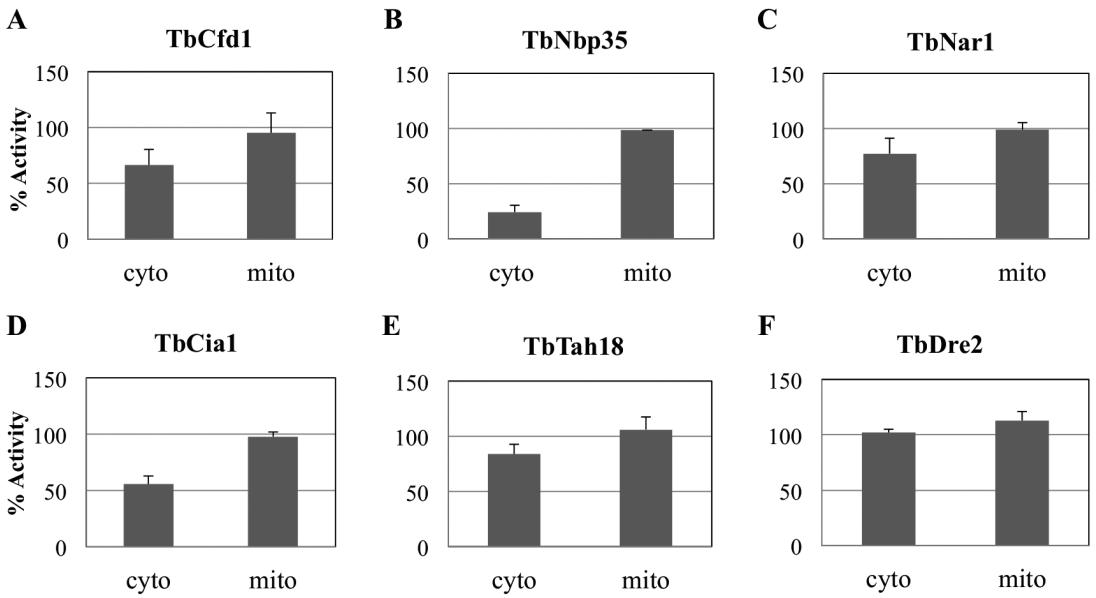

Fig. 3. Cytosolic and mitochondrial aconitase activities after RNAi depletion of CIA candidates. Consequences of single RNAi depletion of the early and middle components of the CIA pathway of PS *T. brucei* were revealed by the measurement of aconitase activities in the mitochondrial and cytosolic fractions. Aconitase activities in these fractions of the non-induced cells have been defined as 100%. The mean and standard deviations of three independent experiments are presented. The aconitase activities were measured after 6 days of RNAi induction.

(Smíd *et al.*, 2006). In TbNbp35, TbCfd1 and TbCia1 RNAi-induced cell lines, the cytosolic but not mitochondrial aconitase activity dropped significantly, compared to the level of the non-induced cells, which was set as 100% (Fig. 3). The strongest effect was observed upon depletion of TbNbp35, which resulted in an 80% drop of the cytosolic activity, while its mitochondrial activity remained unchanged (Fig. 3B). Depletion of TbCfd1 and TbCia1 caused a 40% decrease each (Fig. 3A and D). Cytosolic aconitase activity remained unaffected upon depletion of TbDre2, but we monitored a 20% decrease upon ablation of TbNar1 or TbTah18 (Fig. 3C and E).

CIA components are essential for both PS and BS upon RNAi double knock-down

To tackle the apparent (and unexpected) dispensability of the studied single CIA components, we decided to deplete them more stringently, namely by tandem ablation of several pairs from the early and middle part of the CIA machinery. This is a powerful approach in cases when another protein can (partially) replace the depleted component or when two proteins act in the same pathway (Kafková *et al.*, 2012). The strategy was based on the addition of second gene fragment to the single RNAi knock-down plasmid, resulting into a construct capable, upon RNAi induction, of simultaneous ablation of two target transcripts. Indeed, double depletion of any pair of genes, including those that were individually inert, resulted in detrimental effects for the viability of trypanosomes (Fig. 4). For all the double depletion pairs in the PS cell the growth phenotype emerged on the day 4 after RNAi-induction. Generally, the deleterious growth effects initiated earlier and in a more severe fashion in the BS in comparison to the PS.

We further measured aconitase activity in the cytosol and mitochondria of all constructed RNAi double knock-downs. In line with the severe effect on growth, in the cytosol of all these flagellates enzymatic activity dropped or even disappeared (Fig. 5). The most dramatic decrease was monitored in the PS upon targeting the TbNbp35/TbDre2 pair, for which the activity became undetectable already on day 3 after RNAi induction (Fig. 5B). Hence, an additive effect can be observed, as upon single depletion of TbNbp35 20% activity remained. For both TbTah18/TbDre2 and TbCia1/TbNar1 double knock-downs, cytosolic aconitase decreased by 40% on day 3, followed by an almost complete loss of activity on day 6 (Fig. 5A and C). Taken together, our results showed that the depletion of a single protein did not affect cell growth, but had a moderate effect on cytosolic Fe/S maturation, whereas concomitant targeting of two CIA components was consistently associated with a severe growth defect and a near ablation of the cytosolic aconitase activity. For both TbTah18/TbDre2 and TbCia1/TbNar1 double knock-downs a drop of the mitochondrial aconitase activity has been observed on day 6 (Fig. 5A and C), yet it is much smaller when compared to the strongly reduced activity of its cytosolic counterpart.

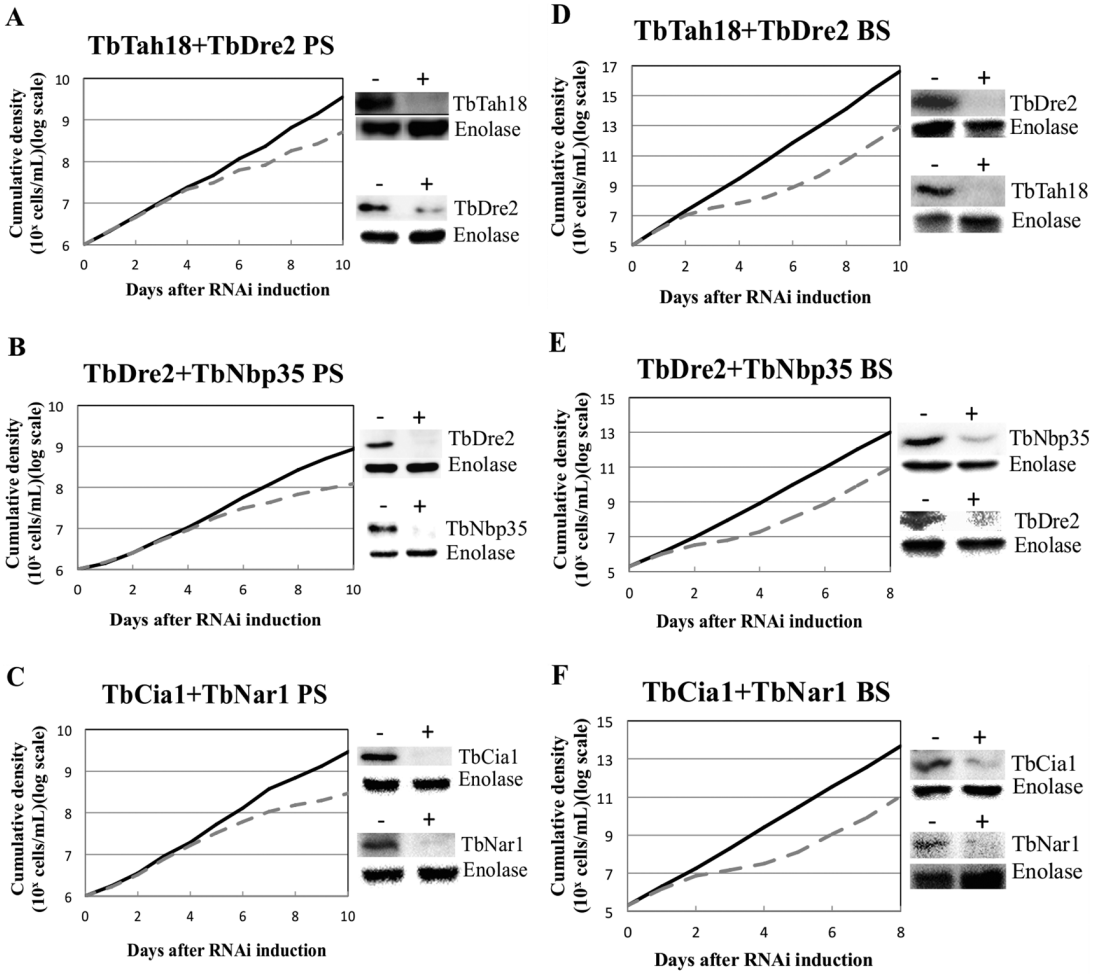

Fig. 4. Essentiality of CIA candidates revealed by double RNAi depletion. Growth of procyclic (PS; A–C) and bloodstream (BS) *T. brucei* RNAi cell-lines (D–F). The curves of the non-induced (solid lines) and RNAi-induced cells (broken lines) are accompanied by respective Western blots showing the depletion of the targeted proteins upon RNAi induction.

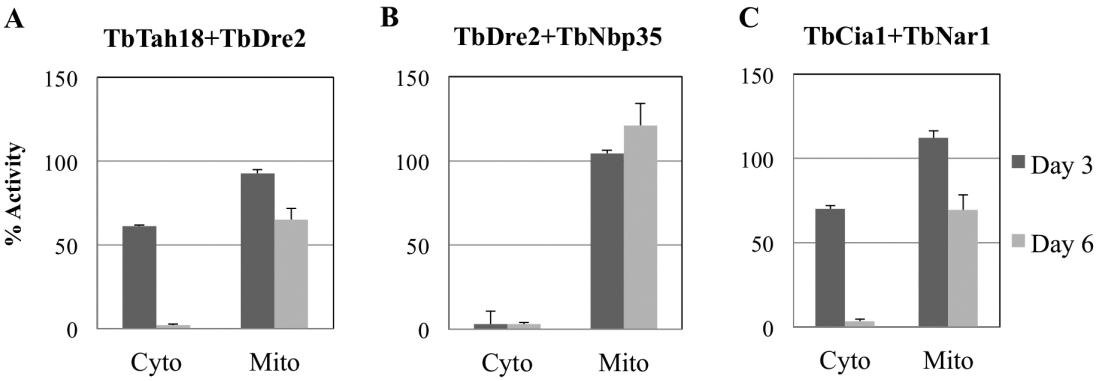

Fig. 5. Cytosolic and mitochondrial aconitase activities after double RNAi depletion of CIA candidates. Consequences of double RNAi depletion of the early and middle components of the CIA pathway were revealed by the measurement of aconitase activities in the mitochondrial and cytosolic fractions. Aconitase activities in these fractions of the non-induced cells have been defined as 100%. The mean and standard deviations of three independent experiments are presented. The aconitase activities were measured after 3 days (darker shade) and 6 days (lighter shade) of RNAi induction.

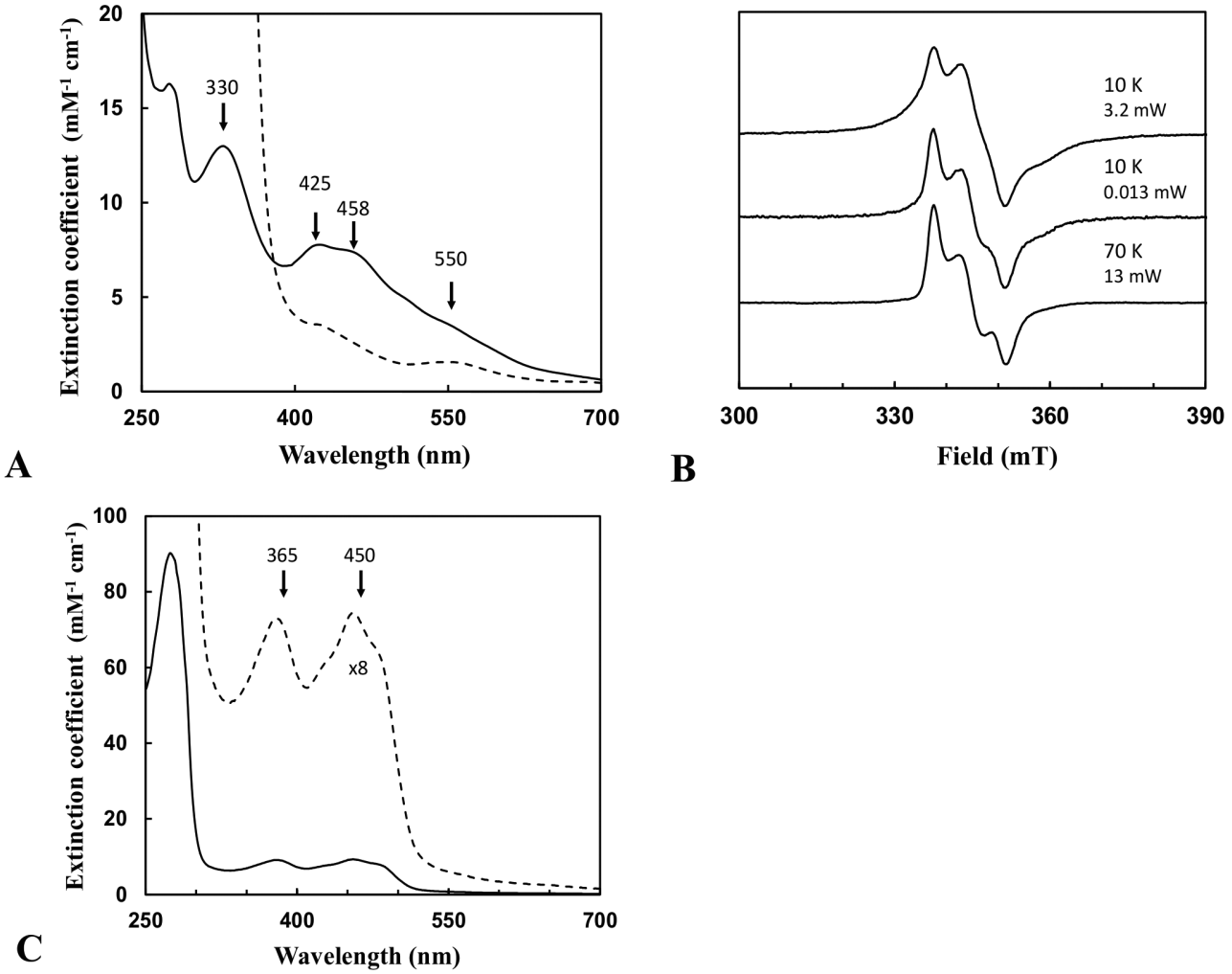

Fig. 6. Spectroscopic features of purified recombinant TbTah18 and TbDre2.
A. UV-VIS spectrum of anaerobically purified TbDre2 (bold line, 0.015 mM) in 25 mM Tris-HCl, 150 mM NaCl, pH 8. The molar extinction coefficients were calculated from the ratios of measured absorbance and the respective protein concentration. The sample was then reduced with 2 mM sodium dithionite (dotted line). The arrows indicate the wavelength of absorbance maxima in nm.
B. EPR spectra of purified TbDre2. Labels at the right side indicate temperature and microwave power at which EPR spectra of 2 mM sodium dithionite-reduced TbDre2 (0.025 mM) were recorded. EPR conditions: microwave frequency 9.460 ± 0.001 GHz; modulation frequency 100 kHz; modulation amplitude 1.25 mT.
C. UV-VIS spectrum of purified TbTah18 (0.025 mM) in 25 mM Tris-HCl, pH 8.0, 150 mM NaCl. Characteristic absorbance maxima are indicated by arrows (wavelength of absorbance maxima in nm). An eightfold magnification is shown as dotted line.

These observations strongly suggest that components of the CIA machinery work in a cooperative manner in *T. brucei*.

Biochemical features of recombinant TbTah18 and TbDre2

TbDre2 lacks the N-terminal *S*-adenosylmethionine (SAM) methyltransferase-like domain of yeast and human Dre2, but retains the two pairs of four conserved cysteine residues in the C-terminal part. The 14.7 kDa His_6-TbDre2 was well expressed in *Escherichia coli* (data not shown) yielding a soluble protein which could be purified (see *Experimental procedures*). TbDre2 had a red-brownish colour and presented an according UV-VIS spectrum with absorbance maxima at 330, 425 and 550 nm (Fig. 6A). The pronounced peak at 330 nm and the discrete shoulders in the 400–550 nm region are similar to those observed for purified plant and human Dre2 proteins (Banci *et al.*, 2013; Bernard *et al.*, 2013). The calculated extinction coefficient, 7.8 mM^{-1} cm^{-1} at 425 nm, is indicative of a single $[2Fe\text{-}2S]^{2+}$ cluster per monomer, as seen for the plant and human Dre2 proteins. Indeed, the EPR spectrum of dithionite-reduced TbDre2 (Fig. 6B) exhibited a characteristic $[2Fe\text{-}2S]^{1+}$ signal at 70 K. A less abundant but distinct, broad EPR signal at 10 K is indicative of the presence of a

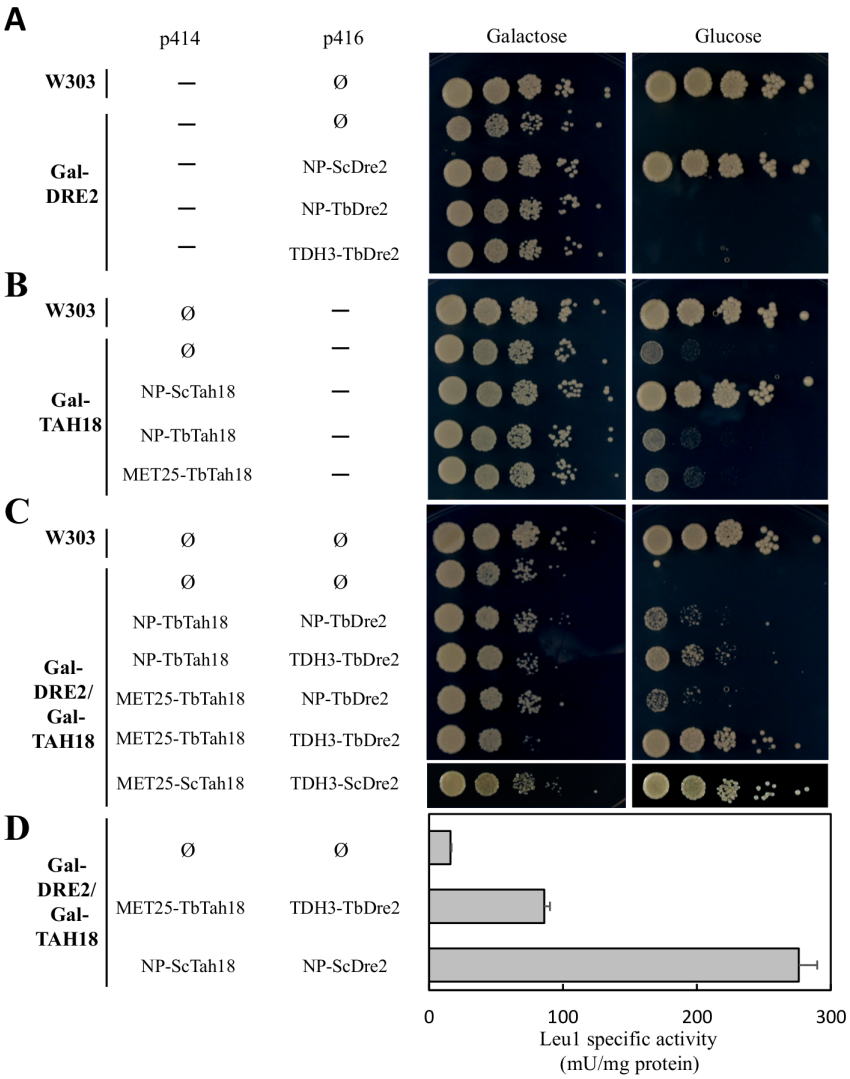

Fig. 7. *T. brucei* Dre2 and Tah18 functionally replace yeast homologues only when expressed in tandem. Plasmids (p414 or p416, as indicated) harbouring no inserts (Ø) or the indicated genes under the control of the strong promoters *MET25* or *TDH3*, and the natural promoter (NP) of *S. cerevisiae DRE2* or *TAH18* were used as indicated.
A–C. Plasmids were transformed into the strains listed at the left: Gal1-10-DRE2, labelled as Gal-DRE2 (A), Gal1-10-TAH18, labelled as Gal-TAH18 (B) and into the double mutant Gal1-10-DRE2/Gal1-10-TAH18, abbreviated as Gal-DRE2/Gal-TAH18 (C). As controls, empty plasmids were transformed into W303 cells. Cells were grown for 40 h in liquid minimal medium supplemented with glucose (2%). After washing, 10-fold serial dilutions were spotted onto agar plates containing minimal medium supplemented with galactose or glucose, and incubated at 30°C for 2 days. The result was reproduced at least three times with independent transformations.
D. Cell extracts of the indicated cells were prepared and the Leu1 activity measured.

small subpopulation of a $[4Fe\text{-}4S]^{1+}$ cluster in addition to the $[2Fe\text{-}2S]^{1+}$ cluster. Together, this analysis shows that TbDre2 is a Fe/S protein.

Upon expression of TbTah18 in *E. coli* (data not shown) a yellowish (oxidized) TbTah18 protein was purified by Ni-NTA affinity chromatography. UV-VIS spectroscopy showed absorbance maxima at 365 and 450 nm (Fig. 6C), compatible with one flavin per TbTah18 molecule. Thus, the diflavin reductase presumably lost part of its chromophores during purification. Taken together, our results indicate that TbDre2 and TbTah18 have biochemical properties similar to their yeast and plant homologues.

Complementation of yeast mutants by T. brucei *CIA components*

For complementation experiments, *T. brucei* Dre2, Tah18, Cfd1, Nbp35, Nar1 and Cia1 genes were PCR-amplified from genomic DNA and cloned into yeast expression vectors under the control of either the natural promoter (NP) of the *S. cerevisiae* CIA genes or the strong yeast promoters *MET25* or *TDH3* (Table S4). Plasmids without insert or plasmids encoding yeast proteins were used as controls. These plasmids were transformed into regulatable yeast Gal-CIA mutants in which the respective CIA gene can be induced in the presence of galactose and repressed by growth with glucose (Pierik *et al.*, 2009). Strong depletion of the yeast CIA proteins in these cells is usually associated with a growth defect, yet the phenotype can be rescued by expression of functionally complementing genes.

Initial experiments using yeast mutants Gal-DRE2 and Gal-TAH18 showed that neither TbDre2 nor TbTah18 were able to complement the growth defect of these cells under depletion conditions (Fig. 7A and B). As expected, full complementation was achieved, when yeast proteins

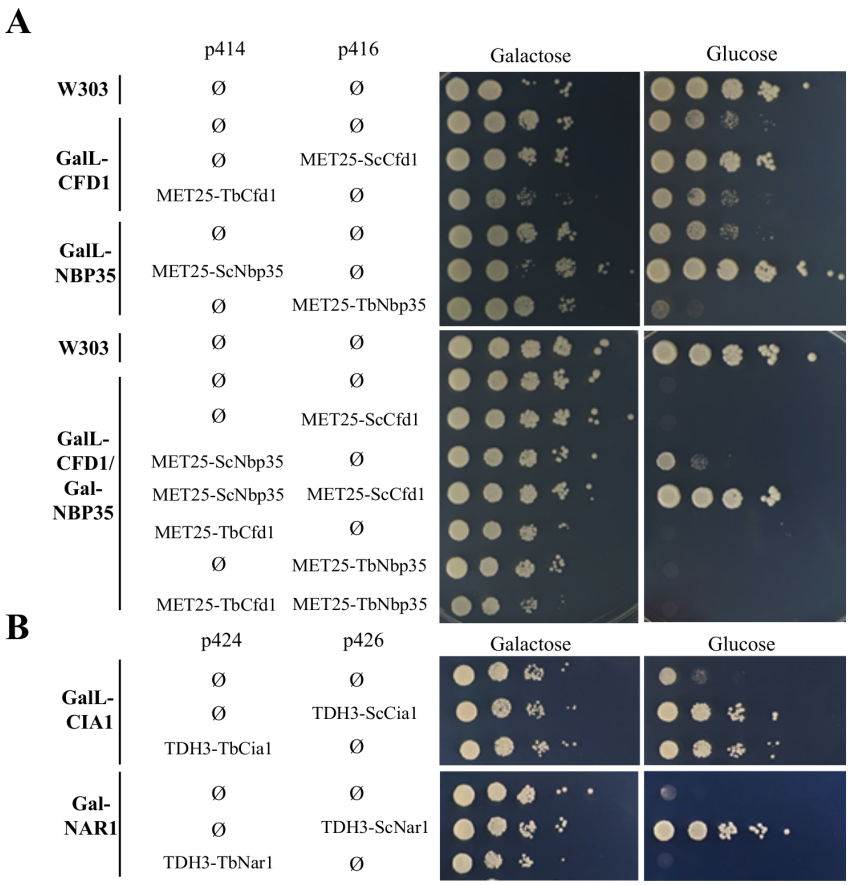

Fig. 8. TbCia1, but not TbCfd1-TbNbp35 and TbNar1 functionally replace their yeast homologues. Experiments were carried out as in Fig. 7.

were expressed at their endogenous levels. In contrast, expression of the parasite proteins did not rescue the cell growth defect, not even after overexpression using strong promoters. Since it is known that Dre2 and Tah18 tightly interact in yeast, plant and human cells (Netz *et al.*, 2010; Banci *et al.*, 2013), we tested the complementation effects after parallel expression of a pair of plasmid-encoded proteins using the double yeast mutant Gal-DRE2/Gal-TAH18 (Fig. 7C). Coexpression of yeast proteins fully rescued the growth phenotype of the double mutant (Fig. 7C, bottom). The complementation by the TbDre2/TbTah18 proteins was tested by expression from various plasmids with promoters of different strengths (Fig. 7C). Coexpression of TbDre2/TbTah18 under yeast endogenous levels partially complemented the cell growth defect. Increased levels of either TbTah18 or TbDre2 did not further improve cell growth, but higher levels of both proteins almost fully restored growth. Measurement of isopropylmalate isomerase (Leu1) activity demonstrated that the ectopic TbDre2/TbTah18 pair not only rescued growth, but also partially restored maturation of this cytosolic Fe/S cluster-containing enzyme (Fig. 7D). Our results demonstrate that TbTah18 and TbDre2 perform an orthologous function to their yeast counterparts.

Next, we addressed whether TbCfd1 and TbNbp35, individually or coexpressed, could functionally replace their yeast homologues in single or double regulatable mutants (GalL-CFD1/Gal-NBP35). As anticipated, the severe growth defect of the single and double mutant cells after depletion on glucose-containing medium was entirely restored by expression of plasmid-encoded yeast Cfd1/Nbp35 (Fig. 8A). From all *T. brucei* CIA proteins analysed, TbCfd1 and TbNbp35 showed the highest identity with the yeast proteins (53% and 48%, relative to Cfd1 and Nbp35 respectively). However, neither TbCfd1 nor TbNbp35 alone or coexpressed rescued the depleted yeast cells. Our results indicate that the scaffold system Cfd1/Nbp35 is organism-specific, and the yeast proteins cannot be complemented by the highly conserved *T. brucei* proteins.

The trypanosomal homologue of Cia1, termed TbCia1, is 35% identical to yeast Cia1 and its sequence similarity is mainly confined to the WD repeats (Srinivasan *et al.*, 2007). This raised the question whether TbCia1 can replace Cia1 in its essential function in the yeast cell (Balk *et al.*, 2005). Remarkably, plasmid-encoded TbCia1 fully complemented the growth defect of yeast cells depleted in endogenous Cia1 (Fig. 8B). Hence, human (Srinivasan *et al.*, 2007) and parasite homologues have the capacity to

functionally replace yeast Cia1 despite moderate primary sequence conservation. We have shown above that the depletion of TbCia1 in *T. brucei* did not affect cell growth whereas double TbCia1/TbNar1 ablation led to cell growth arrest (Fig. 4C and F). TbNar1 has weak similarity to yeast Nar1 (28% identity) and, as shown in Fig. 8B, did not complement Nar1-depleted yeast cells. These findings and the observed lack of rescue by the human Nar1 homologues (Balk *et al*., 2004) indicate that Nar1 is the more critical component of the Nar1–Cia1 interaction in the CIA machinery (Stehling *et al*., 2012).

Discussion

Trypanosoma brucei comprises CIA pathway in its genome, although it was impossible to unequivocally establish the presence of all of its key components based on sequence information only (Basu *et al*., 2013). This may be caused by notorious divergence of kinetoplastid flagellates from other eukaryotes, or by genuine absence of some genes. Therefore, a detailed functional analysis of known CIA components of the early and intermediate part of this pathway is executed.

Ever since the discovery of the first component of the CIA pathway (Roy *et al*., 2003; Hausmann *et al*., 2005), being preeminently studied in the yeast and human cells, many more participants have been progressively appended resulting into a complex machinery (Netz *et al*., 2014). Some components of the CIA pathway are present in related flagellates such as *Leishmania* spp., as well as in other protists. However, some obligatory anaerobic excavates like *Trichomonas vaginalis* and *Giardia intestinalis* not only lack Dre2 (Vernis *et al*., 2009; Jedelský *et al*., 2011; Tsaousis *et al*., 2014) but also the major ISC export machinery candidate Erv1 that is essential for cytosolic Fe/S protein biogenesis in yeast (Lange *et al*., 2001; Tachezy, 2008; Basu *et al*., 2013). These unexpected variations among the highly diverse excavates make *T. brucei* an organism of choice for functional analyses.

Upon individual ablation of the *T. brucei* CIA components by RNAi, most of them proved non-essential under cultivation conditions, except TbNbp35 and TbCfd1. This observation was not compatible with other eukaryotes. To confront this unexpected situation, a RNAi double knockdown strategy was adopted. Rigorous ablation of early and middle part of the pathway, depleting two components in parallel, invariably resulted in growth cessation. This observation indicates that only a strong depletion of the CIA pathway is associated with phenotypical effects in *T. brucei*.

The pathway can be subdivided into components primarily dealing with 'electron transfer chain', 'scaffolds', and 'targeting complex' and are assumed to function as separate modules (Netz *et al*., 2014). Even highly efficient elimination of one of the components of a CIA module is not detrimental for trypanosomes. However, elimination of two partners leads to a severe impairment of the whole 'module', causing downstream disruption of the entire CIA pathway. Biochemical characterization revealed that TbTah18, like its yeast, human and plant homologues, is a diflavin reductase. The TbTah18-depleted trypanosomes remained unaffected because when one component is eliminated from a process comprising two components, it might still work. Nevertheless, if both components are taken out then they hardly might find each other even in the reduced level and also the subsequent process is hampered (TbTah18 → TbDre2 and then TbDre2 → TbNbp35).

According to UV-VIS and EPR spectroscopy purified TbDre2 presents itself as a Fe/S protein carrying a [2Fe-2S] cluster. In comparison to yeast and human Dre2, TbDre2 lacks the entire N-terminal *S*-adenosylmethionine methyltransferase-like domain (Soler *et al*., 2012) but maintains the Fe/S cluster-binding domain, which is essential for viability in yeast (Soler *et al*., 2011). This truncated structure is a common feature of Dre2 in all kinetoplastid flagellates (Fig. S2).

It was of interest to assay the functional complementation of the yeast CIA components by their *T. brucei* counterparts, separated by a long evolutionary distance. The TbTah18-TbDre2 unit efficiently complemented the growth of yeast Tah18-Dre2 double mutant cells proving their function in electron transfer in the *T. brucei* CIA pathway. These results are similar to those recently obtained with *A. thaliana* (Bernard *et al*., 2013), providing further evidence for an exceptional conservation of this essential module of the CIA pathway in evolutionary distant eukaryotes. Indeed, the Tah18-Dre2 module is conserved throughout all eukaryotic super-groups (Ali and Nozaki, 2013; Basu *et al*., 2013) with the exception of the amoebozoan *Entamoeba* sp. (Basu *et al*., 2013) and *Mastigamoeba balamuthi* (Nývltová *et al*., 2013).

Both *T. brucei* CIA scaffold proteins Cfd1 and Nbp35 are well conserved in respect to their yeast and human counterparts, retaining the P-loop motifs and the four conserved cysteine residues (Fig. 1B). However, in spite of the high similarity, TbCfd1 and TbNbp35 failed to complement the function of the yeast scaffolds. Interestingly, *A. thaliana* contains only Nbp35, which works as a homo-oligomeric scaffold without Cfd1. It is therefore not surprising that the *A. thaliana* Nbp35 failed to rescue the growth of yeast cells depleted for Nbp35, but unexpectedly partially rescued the cells ablated for Cfd1 (Bych *et al*., 2008). TbCia1 effectively complements the Cia1-depleted yeast cells, whereas TbNar1 failed to functionally replace its respective yeast orthologue. One possible explanation of the failure of TbNar1 to rescue Nar1-depleted yeast cells is suboptimal interaction of TbNar1 with *S. cerevisiae* Nbp35 and Cia1, which is reminiscent

of rescue experiments in yeast by two human Nar1 homologues (Balk *et al*., 2004).

Trypanosoma brucei undergoes a complex life cycle experiencing two completely different host environments, which is reflected in two biochemically distinct life cycle stages. In the PS the mitochondrion is fully active, containing all the classical respiratory chain complexes (Clarkson *et al*., 1989), while the BS mitochondrion is morphologically reduced lacking the entire respiratory chain (Bringaud *et al*., 2006). We propose that the generally more severe phenotypes observed in the BS trypanosomes reflect these inter-stagial metabolic differences. Since the BS flagellates rely solely on glycolysis, mitochondrial function including the ISC machinery might be impaired, which could make the CIA machinery more susceptible to silencing in these mammalian bloodforms. On the contrary, the fully active organelle the PS cells have a high demand for mitochondrial Fe/S clusters, and perturbation of its ISC pathway is detrimental on its own (Long *et al*., 2011). This notion is further supported by the described upregulation of most CIA components in the BS (Aslett *et al*., 2010). The 'CIA targeting complex' is not elaborated in this study but RNAi against both TbCia2A and TbCia2B lead to a growth phenotype in the BS but not in the PS (S. Basu *et al*., unpubl. results). Collectively, the available data support our hypothesis of an upregulated, quintessential CIA pathway in the sleeping sickness-causing BS flagellates.

Previously, Nbp35 and Cfd1 were shown to be involved in the thiolation of cytosolic tRNAs in yeast and *T. brucei* (Nakai *et al*., 2007; Bruske *et al*., 2009). The strong decrease of the Fe/S cluster-dependent cytosolic aconitase activity upon TbNbp35 and TbCfd1 depletion indicated the involvement of these CIA components in the cytosolic Fe/S cluster assembly. The strong growth phenotypes are likely a consequence of cumulative effects of disrupted tRNA thiolation and the compromised CIA pathway. Ablation of TbDre2, TbTah18 and TbNar1 resulted in a moderate decrease of the cytosolic aconitase, yet this effect became exacerbated in all double RNAi knock-downs. Indeed, dismantling the CIA pathway in such an abrasive manner resulted in a complete loss of the cytosolic aconitase activity in the TbTah18/TbDre2, TbNbp35/TbDre2 and TbCia1/TbNar1 RNAi-treated cells (Fig. 5). In TbTah18/TbDre2 and TbCia1/TbNar1 double RNAi knock-down cells, the mitochondrial aconitase activity also drops, although much less when compared to the cytosolic aconitase (Fig. 5A and C). Possible reason of this effect could be the strongly disarrayed cytosolic Fe/S protein biogenesis affecting genome stability and translation efficiency. The oxidative damage resulting from the severe phenotypes caused by the RNAi double silencing could make the oxidative stress-sensitive mitochondrial aconitase less active, leading to the above-mentioned observation. However, this compartmentalization may not apply vice versa, as two key ISC components were recently localized not only in the mitochondrion, but also in the nucleolus of both PS and BS cells (Kovářová *et al*., 2014). Their precise function remains to be determined.

In a nutshell, the presented data elaborates the CIA pathway for the first time in a highly diverged parasitic protist, shedding light on its remarkably conserved organization.

Experimental procedures

Bioinformatics

Similarity of the CIA candidates has been confirmed using BLAST (Altschul *et al*., 1997) and sequence alignments have been performed by CLUSTALW (Larkin *et al*., 2007). Conserved protein architectures have been analysed with the help of the Conserved Domain Database (Marchler-Bauer *et al*., 2002) and TriTrypDB (Aslett *et al*., 2010).

Trypanosome cell culture and RNAi

Procyclic *T. brucei* 29-13 (Wirtz *et al*., 1999) were grown in SDM-79 (Brun and Schönenberger, 1979) containing 10% fetal bovine serum, 15 μg ml^{-1} geneticin and 50 μg ml^{-1} hygromycin. Bloodstream *T. brucei* 427 (Wirtz *et al*., 1999) were cultivated in HMI-9 medium (Hirumi and Hirumi, 1989) containing 10% fetal bovine serum and 2.5 μg ml^{-1} geneticin. For single RNAi, gene fragments from TbCia1, TbNar1,TbDre2 and TbTah18 were PCR-amplified from the *T. brucei* genomic DNA using primers listed in Table S2. The PCR amplicon was gel-purified, digested with BamHI and XhoI, and ligated into the vector p2T7-177 (Wickstead *et al*., 2002) pre-digested with the same enzymes. For generation of RNAi double knock-down plasmids, gene fragments from TbCia1, TbNbp35 and TbTah18 were obtained using primers listed in Table S3. PCR amplicons were purified, digested with BamHI and SpeI, and ligated into the previously generated single knock-down plasmids, which have been opened with the same enzymes, resulting in p2T7-177 vectors containing the following tandems of gene fragments: TbDre2/TbTah18; TbDre2/TbNbp35 and TbNar1/TbCia1. All generated plasmids were linearized using NotI and electroporated into the PS and BS cells using BTX and Amaxa Nucleofector II electroporators, respectively, as described elsewhere (Wickstead *et al*., 2002; Vondrušková *et al*., 2005). Positive transfectants were selected by clonal dilution using phleomycin as a marker. The PS cell lines containing an inducible RNAi system for knock-down of TbCfd1 and TbNbp35 and corresponding pLew-100-based TbCfd1 and TbNbp35 plasmids were kindly provided by André Schneider (Bruske *et al*., 2009). These plasmids were subsequently electroporated into the BS with puromycin as a selectable marker. RNAi was invariably induced by the addition of tetracycline (1 μg ml^{-1}) to the growth medium and cell densities were measured using a Beckman Coulter Z2 counter every 24 h over a period of 8–10 days after induction.

Yeast strains and plasmids

The *S. cerevisiae* strain W303-1A was used as wild-type (*MATa, ure3-1*, *ade2-1*, *trp1-1*, *his3-11*,*15*, *leu2-3*,*112*). Pre-

viously published promoter-regulatable strains used in this study were: GalL-CIA1 (Netz *et al.*, 2010), Gal-NAR1 (Balk *et al.*, 2004), GalL-CFD1 (Netz *et al.*, 2012), GalL-NBP35 (Netz *et al.*, 2012), Gal1-10 DRE2 (Bernard *et al.*, 2013), Gal1-10 TAH18 (Bernard *et al.*, 2013) and GAL1-10 DRE2/ Gal1-10 TAH18 (Bernard *et al.*, 2013). The double mutant GalL-CFD1/GalL-NBP35 was constructed from the GalL-CFD1 strain in which the endogenous *NBP35* promoter was replaced by homologous recombination with a PCR product containing the NatNT2 resistance marker and the GalL promoter. Correct promoter insertion was confirmed by PCR of chromosomal DNA with primers hybridizing to the flanking regions and the inserted cassette. For plasmid-encoded expression, the *T. brucei* coding regions were PCR-amplified from the *T. brucei* 29-13 genomic DNA. All plasmids used are listed in Table S4. For constructs with natural promoters (NP) of yeast, 450 bp or 518 bp 5′ of the start codons of the yeast *DRE2* or *TAH18* genes, respectively, were used. All constructs were confirmed by sequencing.

Growth complementation and Leu1 activity determination

Growth and transformation was performed as described elsewhere (Pierik *et al.*, 2009). Growth complementation was tested using the regulatable strains described above. After the transformation of plasmids (listed in Table S4) into the respective strains, individual transformants were grown on agar plates containing SC minimal media supplemented with 2% galactose for 2 days at 30°C. Cells were cultivated for 16 or 40 h (i.e. 24 h plus 16 h in fresh medium) in liquid minimal medium supplemented with 2% glucose. After washing, the cells were resuspended to an A_{600} of 0.5 in liquid SC minimal medium containing glucose or galactose. Aliquots of 4 μl and consecutive 10-fold serial dilutions were spotted onto agar plates containing SC minimal media supplemented with 2% galactose or glucose. Plates were incubated for 2 days at 30°C and photographed. In extracts prepared from cells cultivated in liquid SC minimal medium supplemented with glucose for 64 h (i.e. 24 h plus 2 × 16 h in fresh medium), the Leu1 activity was determined as described elsewhere (Pierik *et al.*, 2009).

Protein expression and purification

TbDre2 or TbTah18 were cloned into the first multiple cloning site of the pET-Duet1 vector (Novagen), generating an N-terminal hexa-His-sequence fused to the encoded protein. Single transformant colonies of HMS174 cells were incubated overnight in LB medium at 37°C. A 1% inoculum taken from the pre-culture was used to inoculate Terrific Broth medium. The TbDre2 culture was shifted to 30°C at an A_{600} of 0.5, followed by the addition of IPTG (final concentration 1 mM) and overnight incubation. For TbTah18 the expression was induced similarly but at an A_{600} of 0.8, followed by growth for 3 h at 20°C. Cells were opened through one passage in a high-pressure homogenizer (Avestin) and soluble proteins were obtained by centrifugation for 1 h at 100 000 *g* at 4°C. Proteins were purified by affinity chromatography (Ni-TED for TbDre2 and Ni-NTA for TbTah18) following the manufacturers' instructions. After elution the proteins were rapidly desalted on a Sephadex G25 column equilibrated with 25 mM Tris-HCl and 150 mM NaCl, pH 8.0 (desalting buffer). Purified TbTah18 and TbDre2 were used for spectroscopic analysis.

EPR spectroscopy

The isolated TbDre2 was made anaerobic by passage through a Sephadex G25 column equilibrated with degassed desalting buffer in an anaerobic chamber (Coy), shock-frozen in an EPR tube after 2 min incubation with sodium dithionite (2 mM final concentration) and kept in liquid nitrogen until analysis. EPR spectra were run at cryogenic temperature with a Bruker ESP 300E X-band spectrometer equipped with an Oxford Instrumentals ESR910 helium flow cryostat. The microwave frequency was measured with a Hewlett-Packard 5340A frequency counter.

Subcellular fractionation, aconitase activity measurement, preparations of antibodies and Western blotting

The cytosolic and mitochondrial fractions were acquired by the digitonin fractionation (Smíd *et al.*, 2006). The activity of aconitase in both subcellular compartments was measured spectrophotometrically at 240 nm via the production of *cis*-aconitate from isocitrate (Long *et al.*, 2011).

Polyclonal antibodies against the TbDre2 and TbTah18 proteins were prepared by immunizing a rabbit and a rat at 2 weeks intervals with four subcutaneous injections of 0.5 mg and 0.1 mg of purified recombinant proteins (see above), respectively, with complete (first injection) and incomplete (following injections) Freund's adjuvant. Sera were collected 7 days after the fourth injection and were tested by Western blotting.

For proof of RNAi efficiency, cells were harvested by centrifugation and lysed in hot Laemmli sample buffer. Lysates equivalent to 5×10^6 cells were separated by SDS-PAGE, blotted, and probed with polyclonal rabbit antisera raised against TbDre2, HsCfd1, HsNbp35, ScCia1, ScNar1, TbEnolase and rat antisera against TbTah18 used at dilutions of 1:200, 1:2000, 1:1000, 1:1000, 1:1000, 1:150 000 and 1:200 respectively. The secondary anti-rabbit IgG antibody (1:1000) and anti-rat IgG antibody (1:1000) coupled to alkaline phosphatase or horseradish peroxidase was visualized according to the manufacturer's protocols using the Clarity™ western ECL substrate (Bio-Rad).

Acknowledgements

We thank André Schneider (University of Bern, Bern, Switzerland) for the gift of Nbp35 and Cfd1 RNAi cell lines and constructs. This work was supported by grants from the Grant Agency of the Czech Republic (P305/11/2179), Ministry of Education of the Czech Republic (AMVIS LH12104), the Bioglobe grant CZ.1.07/2.3.00/ 30.0032, and the Praemium Academiae award to J.L., who is also a Fellow of the Canadian Institute for Advanced Research. R.L. acknowledges generous support from Deutsche Forschungsgemeinschaft (SFB 593, GRK 1216), von Behring-Röntgen Stiftung, LOEWE programme of state Hessen, and Max-Planck Gesellschaft. We acknowledge the use of research infrastructure supported

from FP7 under grant agreement No. 316304. A.J.P., R.L., and J.L. designed and directed the study. S.B., D.J.N., A.C.H., N.H., T.J.L. and A.J.P. undertook experiments. S.B., D.J.N., A.J.P., R.L. and J.L. wrote the paper. The authors declare they have no conflicts of interest.

References

Ali, V., and Nozaki, T. (2013) Iron-sulphur clusters, their biosynthesis, and biological functions in protozoan parasites. *Adv Parasitol* **83:** 1–92.

Altschul, S.F., Madden, T.L., Schäffer, A.A., Zhang, J., Zhang, Z., Miller, W., and Lipman, D.J. (1997) Gapped BLAST and PSI-BLAST: a new generation of protein database search programs. *Nucleic Acids Res* **25:** 3389–3402.

Aslett, M., Aurrecoechea, C., Berriman, M., Brestelli, J., Brunk, B.P., Carrington, M., *et al*. (2010) TriTrypDB: a functional genomic resource for the Trypanosomatidae. *Nucleic Acids Res* **38:** D457–D462.

Balk, J., Pierik, A.J., Netz, D.J., Mühlenhoff, U., and Lill, R. (2004) The hydrogenase-like Nar1p is essential for maturation of cytosolic and nuclear iron–sulphur proteins. *EMBO J* **23:** 2105–2115.

Balk, J., Netz, D.J., Tepper, K., Pierik, A.J., and Lill, R. (2005) The essential WD40 protein Cia1 is involved in a late step of cytosolic and nuclear iron-sulfur protein assembly. *Mol Cell Biol* **25:** 10833–10841.

Banci, L., Ciofi-Baffoni, S., Mikolajczyk, M., Winkelmann, J., Bill, E., and Pandelia, M.E. (2013) Human anamorsin binds [2Fe-2S] clusters with unique electronic properties. *J Biol Inorg Chem* **18:** 883–893.

Basu, S., Leonard, J.C., Desai, N., Mavridou, D.A., Tang, K.H., Goddard, A.D., *et al*. (2013) Divergence of Erv1-associated mitochondrial import and export pathways in trypanosomes and anaerobic protists. *Eukaryot Cell* **12:** 343–355.

Bernard, D.G., Netz, D.J., Lagny, T.J., Pierik, A.J., and Balk, J. (2013) Requirements of the cytosolic iron-sulfur cluster assembly pathway in *Arabidopsis*. *Philos Trans R Soc Lond B Biol Sci* **368:** 20120259.

Bringaud, F., Rivière, L., and Coustou, V. (2006) Energy metabolism of trypanosomatids: adaptation to available carbon sources. *Mol Biochem Parasitol* **149:** 1–9.

Brun, R., and Schönenberger (1979) Cultivation and *in vitro* cloning or procyclic culture forms of *Trypanosoma brucei* in a semi-defined medium. *Acta Trop* **36:** 289–292.

Bruske, E.I., Sendfeld, F., and Schneider, A. (2009) Thiolated tRNAs of *Trypanosoma brucei* are imported into mitochondria and dethiolated after import. *J Biol Chem* **284:** 36491–36499.

Bych, K., Netz, D.J., Vigani, G., Bill, E., Lill, R., Pierik, A.J., and Balk, J. (2008) The essential cytosolic iron-sulfur protein Nbp35 acts without Cfd1 partner in the green lineage. *J Biol Chem* **283:** 35797–35804.

Changmai, P., Horáková, E., Long, S., Černotíková-Stříbrná, E., McDonald, L.M., Bontempi, E.J., and Lukeš, J. (2013) Both human ferredoxins equally efficiently rescue ferredoxin deficiency in *Trypanosoma brucei*. *Mol Microbiol* **89:** 135–151.

Clarkson, A.B., Jr, Bienen, E.J., Pollakis, G., and Grady, R.W. (1989) Respiration of bloodstream forms of the parasite *Trypanosoma brucei brucei* is dependent on a plant-like alternative oxidase. *J Biol Chem* **264:** 17770–17776.

Gari, K., Ortiz, A.M., Borel, V., Flynn, H., Skehel, J.M., and Boulton, S.J. (2012) MMS19 links cytoplasmic iron-sulfur cluster assembly to DNA metabolism. *Science* **337:** 243–245.

Hausmann, A., Netz, D.J., Balk, J., Pierik, A.J., Mühlenhoff, U., and Lill, R. (2005) The eukaryotic P loop NTPase Nbp35: an essential component of the cytosolic and nuclear iron-sulfur protein assembly machinery. *Proc Natl Acad Sci USA* **102:** 3266–3271.

Hirumi, H., and Hirumi, K. (1989) Continuous cultivation of *Trypanosoma brucei* blood stream forms in a medium containing a low concentration of serum protein without feeder cell layers. *J Parasitol* **75:** 985–989.

Jedelský, P.L., Doležal, P., Rada, P., Pyrih, J., Smíd, O., Hrdý, I., *et al*. (2011) The minimal proteome in the reduced mitochondrion of the parasitic protist *Giardia intestinalis*. *PLoS ONE* **6:** e17285.

Kafková, L., Ammerman, M.L., Faktorová, D., Fisk, J.C., Zimmer, S.L., Sobotka, R., *et al*. (2012) Functional characterization of two paralogs that are novel RNA binding proteins influencing mitochondrial transcripts of *Trypanosoma brucei*. *RNA* **18:** 1846–1861.

Kispal, G., Csere, P., Prohl, C., and Lill, R. (1999) The mitochondrial proteins Atm1p and Nfs1p are essential for biogenesis of cytosolic Fe/S proteins. *EMBO J* **18:** 3981–3989.

Klinge, S., Hirst, J., Maman, J.D., Krude, T., and Pellegrini, L. (2007) An iron-sulfur domain of the eukaryotic primase is essential for RNA primer synthesis. *Nat Struct Mol Biol* **14:** 875–877.

Kovářová, J., Horáková, E., Changmai, P., Vancová, M., and Lukeš, J. (2014) Mitochondrial and nucleolar localization of cysteine desulfurase Nfs and the scaffold protein Isu in *Trypanosoma brucei*. *Eukaryot Cell* **13:** 353–362.

Lange, H., Lisowsky, T., Gerber, J., Muhlenhoff, U., Kispal, G., and Lill, R. (2001) An essential function of the mitochondrial sulfhydryl oxidase Erv1p/ALR in the maturation of cytosolic Fe/S proteins. *EMBO Rep* **2:** 715–720.

Larkin, M.A., Blackshields, G., Brown, N.P., Chenna, R., McGettigan, P.A., McWilliam, H., *et al*. (2007) Clustal W and Clustal X version 2.0. *Bioinformatics* **23:** 2947–2948.

Lill, R. (2009) Function and biogenesis of iron-sulphur proteins. *Nature* **460:** 831–838.

Long, S., Changmai, P., Tsaousis, A.D., Skalický, T., Verner, Z., Wen, Y.Z., *et al*. (2011) Stage-specific requirement for Isa1 and Isa2 proteins in the mitochondrion of *Trypanosoma brucei* and heterologous rescue by human and *Blastocystis* orthologues. *Mol Microbiol* **81:** 1403–1418.

Lukeš, J., Hashimi, H., and Zíková, A. (2005) Unexplained complexity of the mitochondrial genome and transcriptome in kinetoplastid flagellates. *Curr Genet* **48:** 277–299.

Marchler-Bauer, A., Panchenko, A.R., Shoemaker, B.A., Thiessen, P.A., Geer, L.Y., and Bryant, S.H. (2002) CDD: a database of conserved domain alignments with links to domain three-dimensional structure. *Nucleic Acids Res* **30:** 281–283.

Montagnes, D., Roberts, E., Lukeš, J., and Lowe, C. (2012) The rise of model protozoa. *Trends Microbiol* **20:** 184–191.

Nakai, Y., Nakai, M., Lill, R., Suzuki, T., and Hayashi, H. (2007) Thio modification of yeast cytosolic tRNA is an

iron-sulfur protein-dependent pathway. *Mol Cell Biol* **27:** 2841–2847.
Netz, D.J., Pierik, A.J., Stümpfig, M., Mühlenhoff, U., and Lill, R. (2007) The Cfd1-Nbp35 complex acts as a scaffold for iron-sulfur protein assembly in the yeast cytosol. *Nat Chem Biol* **3:** 278–286.
Netz, D.J., Stümpfig, M., Doré, C., Mühlenhoff, U., Pierik, A.J., and Lill, R. (2010) Tah18 transfers electrons to Dre2 in cytosolic iron-sulfur protein biogenesis. *Nat Chem Biol* **6:** 758–765.
Netz, D.J., Stith, C.M., Stümpfig, M., Köpf, G., Vogel, D., Genau, H.M., *et al*. (2011) Eukaryotic DNA polymerases require an iron-sulfur cluster for the formation of active complexes. *Nat Chem Biol* **8:** 125–132.
Netz, D.J., Pierik, A.J., Stümpfig, M., Bill, E., Sharma, A.K., Pallesen, L.J., *et al*. (2012) A bridging [4Fe-4S] cluster and nucleotide binding are essential for function of the Cfd1-Nbp35 complex as a scaffold in iron-sulfur protein maturation. *J Biol Chem* **287:** 12365–12378.
Netz, D.J., Mascarenhas, J., Stehling, O., Pierik, A.J., and Lill, R. (2014) Maturation of cytosolic and nuclear iron-sulfur proteins. *Trends Cell Biol* **24:** 303–312.
Nývltová, E., Šuták, R., Harant, K., Šedinová, M., Hrdy, I., Paces, J., *et al*. (2013) NIF-type iron-sulfur cluster assembly system is duplicated and distributed in the mitochondria and cytosol of *Mastigamoeba balamuthi*. *Proc Natl Acad Sci USA* **110:** 7371–7376.
Paris, Z., Changmai, P., Rubio, M.A., Zíková, A., Stuart, K.D., Alfonzo, J.D., and Lukeš, J. (2010) The Fe/S cluster assembly protein Isd11 is essential for tRNA thiolation in *Trypanosoma brucei*. *J Biol Chem* **285:** 22394–22402.
Pierik, A.J., Netz, D.J., and Lill, R. (2009) Analysis of iron-sulfur protein maturation in eukaryotes. *Nat Protoc* **4:** 753–766.
Roche, B., Aussel, L., Ezraty, B., Mandin, P., Py, B., and Barras, F. (2013) Iron/sulfur proteins biogenesis in prokaryotes: formation, regulation and diversity. *Biochim Biophys Acta* **1827:** 455–469.
Roy, A., Solodovnikova, N., Nicholson, T., Antholine, W., and Walden, W.E. (2003) A novel eukaryotic factor for cytosolic Fe-S cluster assembly. *EMBO J* **22:** 4826–4835.
Rudolf, J., Makrantoni, V., Ingledew, W.J., Stark, M.J., and White, M.F. (2006) The DNA repair helicases XPD and FancJ have essential iron-sulfur domains. *Mol Cell* **23:** 801–808.
Saas, J., Ziegelbauer, K., Von Haeseler, A., Fast, B., and Boshart, M. (2000) A developmentally regulated aconitase related to iron-regulatory protein-1 is localized in the cytoplasm and in the mitochondrion of *Trypanosoma brucei*. *J Biol Chem* **275:** 2745–2755.
Sipos, K., Lange, H., Fekete, Z., Ullmann, P., Lill, R., and Kispal, G. (2002) Maturation of cytosolic iron-sulfur proteins requires glutathione. *J Biol Chem* **277:** 26944–26949.
Smíd, O., Horáková, E., Vilímová, V., Hrdy, I., Cammack, R., Horváth, A., *et al*. (2006) Knock-downs of iron-sulfur cluster assembly proteins IscS and IscU down-regulate the active mitochondrion of procyclic *Trypanosoma brucei*. *J Biol Chem* **281:** 28679–28686.
Soler, N., Delagoutte, E., Miron, S., Facca, C., Baïlle, D., d'Autreaux, B., *et al*. (2011) Interaction between the reductase Tah18 and highly conserved Fe-S containing Dre2 C-terminus is essential for yeast viability. *Mol Microbiol* **82:** 54–67.
Soler, N., Craescu, C.T., Gallay, J., Frapart, Y.M., Mansuy, D., Raynal, B., *et al*. (2012) A S-adenosylmethionine methyltransferase-like domain within the essential, Fe-S-containing yeast protein Dre2. *FEBS J* **279:** 2108–2119.
Srinivasan, V., Netz, D.J., Webert, H., Mascarenhas, J., Pierik, A.J., Michel, H., and Lill, R. (2007) Structure of the yeast WD40 domain protein Cia1, a component acting late in iron-sulfur protein biogenesis. *Structure* **15:** 1246–1257.
Srinivasan, V., Pierik, A.J., and Lill, R. (2014) Crystal structures of nucleotide-free and glutathione-bound mitochondrial ABC transporter Atm1. *Science* **343:** 1137–1140.
Stehling, O., Vashisht, A.A., Mascarenhas, J., Jonsson, Z.O., Sharma, T., Netz, D.J., *et al*. (2012) MMS19 assembles iron-sulfur proteins required for DNA metabolism and genomic integrity. *Science* **337:** 195–199.
Stehling, O., Mascarenhas, J., Vashisht, A.A., Sheftel, A.D., Niggemeyer, B., Rösser, R., *et al*. (2013) Human CIA2A-FAM96A and CIA2B-FAM96B integrate iron homeostasis and maturation of different subsets of cytosolic-nuclear iron-sulfur proteins. *Cell Metab* **18:** 187–198.
Tachezy, J. (ed.) (2008) *Hydrogenosomes and Mitosomes: Mitochondria of Anaerobic Eukaryotes*. Berlin, Heidelberg: Springer Berlin Heidelberg.
Tsaousis, A.D., Gentekaki, E., Eme, L., Gaston, D., and Roger, A.J. (2014) Evolution of the cytosolic iron-sulfur cluster assembly machinery in *Blastocystis* species and other microbial eukaryotes. *Eukaryot Cell* **13:** 143–153.
Vernis, L., Facca, C., Delagoutte, E., Soler, N., Chanet, R., Guiard, B., *et al*. (2009) A newly identified essential complex, Dre2-Tah18, controls mitochondria integrity and cell death after oxidative stress in yeast. *PLoS ONE* **4:** e4376.
Vondrušková, E., Van Den Burg, J., Zíková, A., Ernst, N.L., Stuart, K., Benne, R., and Lukeš, J. (2005) RNA interference analyses suggest a transcript-specific regulatory role for mitochondrial RNA-binding proteins MRP1 and MRP2 in RNA editing and other RNA processing in *Trypanosoma brucei*. *J Biol Chem* **280:** 2429–2438.
Wickstead, B., Ersfeld, K., and Gull, K. (2002) Targeting of a tetracycline-inducible expression system to the transcriptionally silent minichromosomes of *Trypanosoma brucei*. *Mol Biochem Parasitol* **125:** 211–216.
Wirtz, E., Leal, S., Ochatt, C., and Cross, G.A. (1999) A tightly regulated inducible expression system for conditional gene knock-outs and dominant-negative genetics in *Trypanosoma brucei*. *Mol Biochem Parasitol* **99:** 89–101.
Yeeles, J.T., Cammack, R., and Dillingham, M.S. (2009) An iron-sulfur cluster is essential for the binding of broken DNA by AddAB-type helicase-nucleases. *J Biol Chem* **284:** 7746–7755.

Supporting information

Additional supporting information may be found in the online version of this article at the publisher's web-site.